RSC Advances

PAPER

View Article Online
View Journal | View Issue

Cite this: *RSC Adv.*, 2019, **9**, 740

Solvothermal water-diethylene glycol synthesis of $LiCoPO_4$ and effects of surface treatments on lithium battery performance†

Min Zhang, [a] Nuria Garcia-Araez, [a] Andrew L. Hector, *[a] John R. Owen,[a] Robert G. Palgrave, [b] Michael G. Palmer[a] and Samantha Soulé[a]

Received 23rd October 2018
Accepted 16th December 2018

DOI: 10.1039/c8ra08785g

rsc.li/rsc-advances

Olivine-structured $LiCoPO_4$ is prepared *via* a facile solvothermal synthesis, using various ratios of water/diethylene glycol co-solvent, followed by thermal treatment under Ar, air, $5\%H_2/N_2$ or NH_3. The diethylene glycol plays an important role in tailoring the particle size of $LiCoPO_4$. It is found that using a ratio of water/diethylene glycol of 1 : 6 (v/v), $LiCoPO_4$ is obtained with a homogenous particle size of ~150 nm. The bare $LiCoPO_4$ prepared after heating in Ar exhibits high initial discharge capacity of 147 mA h g^{-1} at 0.1C with capacity retention of 70% after 40 cycles. This is attributed to the enhanced electronic conductivity of $LiCoPO_4$ due to the presence of Co_2P after firing under Ar. The effects of carbon, TiN and RuO_2 coating are also examined. Contrary to other studies, it is found that the solvothermally synthesised $LiCoPO_4$ samples produced here do not require conductive coatings to achieve good performance.

Introduction

Development of energy storage and conversion devices is vital to address the increasing energy crisis and ecological concerns in the 21st century.[1] Although a variety of renewable energy technologies such as solar cells, fuel cells and biofuels have been developed,[2–5] the need for efficient, cheap and reliable storage devices is still pressing when using renewable energies.[5] Electrical energy storage like lithium batteries and supercapacitors are effective strategies in making the energy output much cleaner.[6–8] As one of the most efficient energy storage devices, lithium-ion batteries (LIBs) are used in portable electronic devices and large-scale electric vehicles[9–12] due to their high energy density, high power density and light weight compared with conventional batteries.[13–15] The olivine-structured $LiMPO_4$ (M = Fe, Mn, Co, Ni) phases have been intensively investigated as cathode materials for LIBs,[15–18] especially $LiFePO_4$ which has been successfully commercialised.[19–24] $LiCoPO_4$ has also attracted significant attention due to its high redox potential (4.8 V *vs.* Li/Li^+) and high theoretical capacity (167 mA h g^{-1}), making it a promising future cathode material for high-voltage LIBs.[25–30] However, use of $LiCoPO_4$ as a cathode in practical applications has been hindered by its unsatisfactory cycle stability and rate capability, which could be mainly attributed to its low electronic conductivity[17,31–36] and poor Li^+ ionic conductivity[36–41] relating to the one-dimensional ion transport channels,[42] as well as to the decomposition of electrolytes under high potentials.[43]

Efforts to overcome the low electronic and ionic conductivity of $LiCoPO_4$ have included: (1) size reduction and morphology control, decreasing the particle size of $LiCoPO_4$ or tailoring its crystal growth orientation along the *a–c* plane to decrease the diffusion length of lithium ions in the insertion/extraction process;[44,45] (2) surface modification (*e.g.* carbon coating), to enhance the electronic conductivity of the composite electrode by forming a conductive network among the $LiCoPO_4$ particles;[42,46] (3) ion doping with cations on either Li or Co sites to enhance the intrinsic electronic/ionic conductivity of $LiCoPO_4$ although the mechanism is still in controversy.[29,47] Among these approaches, the combination of size reduction and conductive agent coating (*e.g.* carbon coating) is regarded as an effective method to enhance the specific capacity and rate capability of $LiCoPO_4$ cathode.[48] Reducing the particle size of $LiCoPO_4$ to the nanometer size range can shorten the Li ion transport distance, and thus reduce the time required for Li ion diffusion within the bulk $LiCoPO_4$ material. Carbon coating not only improves the surface electrical conductivity of $LiCoPO_4$ composite, which alleviates electrode polarization, but also provides effective protection from chemical attack by HF produced *via* electrolyte decomposition at high potentials in $LiPF_6$ based electrolytes.[48] Metal oxides[30,49–52] and metal nitrides[53–56] have been combined with other electrode materials to form structured composites with improved conductivity and stability. TiN and RuO_2 are

[a]*School of Chemistry, University of Southampton, Highfield, Southampton SO17 1BJ, UK. E-mail: A.L.Hector@soton.ac.uk*

[b]*Department of Chemistry, University College London, 20 Gordon Street, London WC1H 0AJ, UK*

† Electronic supplementary information (ESI) available. See DOI: 10.1039/c8ra08785g

suitable for this purpose as they have good electrical conductivity, and good chemical and thermal stability.[53,57]

It is important to develop facile, easily scalable and controllable, time and energy saving synthetic routes to produce $LiCoPO_4$ with good electrochemical performance.[25] Various synthesis methods such as hydrothermal/solvothermal syntheses,[42,44] sol–gel processes[58,59] and solid-state reactions[60,61] have been proposed. Hydrothermal/solvothermal synthesis is facile and easily scalable, with mild reaction conditions and advantages of producing nanomaterials with controllable particle sizes and morphologies.[62] Mixing an organic solvent and water as a co-solvent has been employed in the solvothermal synthesis of $LiCoPO_4$.[44,45,62–64] The solvent mixture can be beneficial for effectively tailoring the particle size of $LiCoPO_4$ due to the high viscosity of the organic solvent,[62,63] and the water component can promote the dissolution of the reagents.[62] However, optimisation of solvothermal conditions to achieve $LiCoPO_4$ cathodes with good specific capacity and cycle performance is still challenging.

Herein, a novel, simple and fast solvothermal approach towards high-performance $LiCoPO_4$ at relatively low temperatures (180 °C) using diethylene glycol (DEG) as a co-solvent is presented, followed by thermal treatment under Ar, air, 5%H_2/N_2 or NH_3. Surface modification of $LiCoPO_4$ with conductive agents like TiN, RuO_2 and carbon has been investigated. Unusually in this work the electrochemical performance of samples produced by this method does not require the use of conductive coatings (*e.g.* carbon) to achieve good electrochemical performance.

Experimental

$LiCoPO_4$ was prepared under solvothermal conditions. We previously reported the phase behaviour during charging of a sample made in this way.[65] LiOH (0.359 g, 0.015 mol, Sigma Aldrich) was dissolved/dispersed in 45 ml deionised water/diethylene glycol (H_2O/DEG) mixture, then H_3PO_4 aqueous solution (0.344 cm^3, 0.005 mol, 85.3 wt% assay, Fisher Scientific) was added. $CoSO_4 \cdot 7H_2O$ (1.405 g, 0.005 mol, ≥ 99% purity, Sigma Aldrich) was dissolved in 25 ml H_2O/DEG mixture and added slowly to the LiOH solution with constant stirring, during which time a blue/purple suspension formed. The volume ratio of H_2O/DEG was set as pure H_2O, 6 : 1, 3 : 1, 1 : 1, 1 : 3, 1 : 6 and pure DEG. The precursor solution was heated in a Parr 4748 Teflon-lined autoclave (125 cm^3) at 180 °C for 10 h. The precipitate was then washed with deionized water and ethanol, and dried at 80 °C for 5 h under vacuum. The resulting material was heated at 5 °C min^{-1} to 600 °C and maintained for 3 h under Ar, air, NH_3 or 5% H_2/N_2 to crystallise $LiCoPO_4$.

To obtain carbon or RuO_2 coated $LiCoPO_4$ the uncrystallised or pre-fired $LiCoPO_4$, (0.3 g, 1.87 mmol) was manually ground in a pestle and mortar with sucrose ($C_6H_{12}O_6$, 0.0375 g, 0.11 mmol, Fisher Scientific) or ruthenium(III) chloride hydrate ($RuCl_3 \cdot xH_2O$, 0.0246 g, 0.12 mmol, Sigma Aldrich) to obtain a uniform mix that was then heated under Ar as described above. The products were black powders and were ground before further characterisation. TiN modified $LiCoPO_4$ powders were prepared using a propylamine cross-linking sol–gel process[53,66–68] under nitrogen using glove box or Schlenk line conditions. $Ti(NMe_2)_4$ (0.21 cm^3, 0.9 mmol, prepared from $TiCl_4$ and $LiNMe_2$) was dissolved in dry THF (7.5 cm^3, distilled from sodium/benzophenone), and added to 0.5 g dry $LiCoPO_4$ powder. $^nPrNH_2$ (0.15 cm^3, 1.8 mmol, distilled from BaO) was slowly added. The solution gradually changed colour from yellow to red-orange. The suspension was stirred at room temperature for ~16 h and dried *in vacuo* to form a sticky powder. This was heated under Ar or NH_3 as described above for $LiCoPO_4$ samples.

Powder X-ray diffraction used a Bruker D2 Phaser with CuK_α radiation, and data was fitted using the GSAS package.[69] Scanning electron microscopy (SEM) used a JEOL JSM-6500F (30 kV). Transmission electron microscopy (TEM) used a FEI Tecnai T12 (120 kV). Brunauer–Emmett–Teller (BET) surface area and pore size distribution measurements *via* N_2 physisorption analysis were carried out with a Micromeritics TriStar II analyser. Electrochemical testing used a Biologics VMP-2 multichannel potentiostat. X-ray photoelectron spectroscopy (XPS) was collected with a two chamber Thermo K-alpha spectrometer with a monochromated Al K-alpha X-ray source (1486.6 eV) in constant analyser energy mode. Sample charging was prevented by use of a dual beam flood gun. X-rays were focused to a 400 μm spot at the sample surface. High resolution core peak spectra were recorded at 50 eV pass energy. Spectra were analysed using Casa XPS software. The binding energy scale was calibrated from the carbon at 285.0 eV. Core peaks were analysed with a nonlinear Shirley-type background.[70] The peak positions and areas were optimized using a weighted least-square fitting method with 70% Gaussian and 30% Lorentzian line shapes. Several spectral analyses were applied at different positions for each sample to ensure the results were statistically reliable. Electronic and ionic conductivity was determined from the current–voltage measurement and electrochemical impedance spectroscopy on gold-coated sintered $LiCoPO_4$ disks (11 mm in diameter and ~0.5 mm in thickness).[31,71,72] Current–voltage plots were collected at 20 mV s^{-1} over the range of −0.3 to +0.3 V (or larger voltage ranges) at room temperature. Electrochemical impedance spectroscopies were collected at 500 mV in the frequency range of 0.1 Hz to 200 kHz at room temperature.

Electrodes for use in lithium half cells were prepared by manually mixing the $LiCoPO_4$ or TiN/carbon/RuO_2 coated $LiCoPO_4$ powders (75 wt%) with acetylene black (Shawinigan Black, 20 wt%) and polytetrafluoroethylene (6C–N, DuPont, 5 wt%) in a pestle and mortar. The resulting solid paste was hand rolled (Durston Rolling Mill) into a film of ~90 μm thickness and cut into circular disks with diameter of 11 mm. The pellet was then dried at 120 °C *in vacuo* for 12 h to obtain the cathode with a typical mass of ~0.022 g. Swagelok cells were assembled in an argon-filled glove box with lithium foil (Rockwood Lithium GmbH) anodes and glass microfiber filter (Whatman, GF/F grade) separators soaked in 8 drops (~0.4 ml) of 1 mol dm^{-3} $LiPF_6$ in ethylene carbonate/ethylmethyl carbonate (EC : EMC = 3 : 7 in weight) electrolyte (BASF, LP57). Galvanostatic testing was carried out at 25 °C at various

rates of charge/discharge (*e.g.* 0.1C for a theoretical specific capacity of 167 mA h g^{-1} corresponds to a specific current of 16.7 mA g^{-1}) within the voltage range of 3.5–5 V (*vs.* Li/Li^+).

Results and discussion

$LiCoPO_4$ samples were prepared by a solvothermal method. First, we present a systematic study on the effect of the solvents and heating environment to optimise the solvothermal conditions. Then, $LiCoPO_4$ samples were coated with TiN, carbon or RuO_2 with a variety of processing conditions and thicknesses to determine whether the expected conductivity enhancement and increased surface stability improved the electrochemical behaviour of the materials.

Effect of solvent on $LiCoPO_4$ morphology in solvothermal synthesis

Uncoated $LiCoPO_4$ samples were produced using H_2O/DEG solvent mixtures with various volume ratios, followed by firing at 600 °C in an Ar environment, to determine the effect of solvents on their morphologies. The volume ratio of H_2O/DEG in solvothermal synthesis was set as pure H_2O, 6 : 1, 3 : 1, 1 : 1, 1 : 3, 1 : 6 and pure DEG, which corresponds to samples defined as LCP-H_2O(Ar), LCP-6 : 1(Ar), LCP-3 : 1(Ar), LCP-1 : 1(Ar), LCP-1 : 3(Ar), LCP-1 : 6(Ar), LCP-DEG(Ar), respectively. The heating temperature affects purity, crystallite/particle size distribution and specific capacity of $LiCoPO_4$.[53] Most successful previous studies produce $LiCoPO_4$ samples at 550–700 °C,[45,73–75] and in this study samples were fired at 600 °C.

The SEM images (Fig. 1) show the morphologies of $LiCoPO_4$ samples obtained using various ratios of H_2O/DEG. The particle size of $LiCoPO_4$ decreased from ~10 μm to ~80 nm with increasing DEG content (Fig. 1a–g), and its BET surface area increased from 1.8 to 22.6 m^2 g^{-1} (Fig. 1h). As the ratio of H_2O/DEG decreases to less than 1 : 3, the particle size distribution of $LiCoPO_4$ becomes homogeneous (Fig. 1f and g). $LiCoPO_4$ particles readily grow to large sizes in hydrothermal (pure water) synthesis.[42,76–78] The pore size distribution of $LiCoPO_4$ samples obtained using various ratios of H_2O/DEG were investigated *via* N_2 physisorption analysis (ESI, Fig. S1†). The isotherms of $LiCoPO_4$ samples belong to the type-II, which is reflective of nonporous or macroporous structure. The density functional theory (DFT) pore size distributions calculated from the adsorption curves reveal that the main pore sizes of $LiCoPO_4$ samples are 4–20 nm. These mesopores are created by the interfaces between nonporous $LiCoPO_4$ particles. The control of particle sizes in solvent mixtures has been attributed to the increased viscosity of the solvent mixture when increasing DEG concentration, which can reduce mass transport to growing crystallite surfaces, thus results in decreasing $LiCoPO_4$ particle size.[63,79] Also, the solubility of the precursors decreases as the solvent mix becomes less polar, which increases the nucleation rate during the solvothermal process.[45] For a given amount of precursor, more nuclei means less matter for each nucleus.[45,80] Therefore, larger nucleation rate in solvothermal process could result in smaller $LiCoPO_4$ particle size.

Our previous review on $LiCoPO_4$ inferred that good rate capability is more likely to be achieved by $LiCoPO_4$ with particle size less than 200 nm.[25] For example, Wei *et al.* synthesized carbon coated $LiCoPO_4$ with particle size of 150 nm *via* a microwave heating method. This nanostructured $LiCoPO_4$ provides a specific capacity of 144 mA h g^{-1} at 0.1C, with reasonable rate capability of 116, 90 and 71 mA h g^{-1} at 5, 10 and 20C, respectively.[81] In this work, sample LCP-1 : 6(Ar) and LCP-DEG(Ar) showed homogeneous particle size distribution with nanoparticle of less than 200 nm. This small particle size can reduce the length of Li-ion migration paths, and facilitate easier Li-ion transfer in $LiCoPO_4$ crystals, thus enhancing the rate performance of LIBs.[45,79,82] However, nanosized $LiCoPO_4$ particles with high surface area can enlarge the electrode/electrolyte interface area, which leads to undesirable electrode/electrolyte by-reactions, thus resulting in a poor cycle stability.[20] Hence, sample LCP-1 : 6(Ar) with particle size of ~150 nm and a relatively small surface area of 5.4 m^2 g^{-1} (compared to LCP-DEG(Ar) with surface area of 22.6 m^2 g^{-1}) was chosen for the following studies.

Effect of heating environment on bare $LiCoPO_4$

Ar or air are typical heating environments in thermal treatment to crystallise $LiCoPO_4$, but the intrinsic role and effects of various heating gases on $LiCoPO_4$ has still not been fully ascertained and remains controversial.[25] NH_3 and 5% H_2/N_2 are typical heating gases to coat TiN and carbon onto electrode materials.[25,48,53] Thus, it is important to evaluate whether heating in NH_3 or 5% H_2/N_2 caused a deterioration in the $LiCoPO_4$ properties. In this section, uncoated $LiCoPO_4$ samples were produced by using the 1 : 6 (v/v) H_2O/DEG co-solvent optimised above, and fired at 600 °C in Ar, air, 5% H_2/N_2 or NH_3 to determine the effect of heating environment on their behaviour. Scheme 1 shows the labels used for different samples.

The X-ray diffraction peaks of the resulting $LiCoPO_4$ samples (Fig. 2) were consistent with the standard olivine $LiCoPO_4$ (JCPDS card no. 85–0002, space group *Pnma*) as expected. Table S1† shows the crystallographic data of $LiCoPO_4$ samples. The Rietveld fits[83] to this XRD data (ESI, Fig. S2†) resulted in similar lattice parameters (ESI, Table S1†) to those in the literature for $LiCoPO_4$ indicating that the heating environment did not affect the crystal structure of $LiCoPO_4$.[84] The Lorentzian peak broadening in the Rietveld fit indicated average $LiCoPO_4$ crystallite sizes of 119–132 nm. These were consistent with TEM (Fig. 3) and SEM (ESI, Fig. S3†) images of $LiCoPO_4$ fired in Ar, air, 5% H_2/N_2 and NH_3, which showed particle sizes of ~150 nm. No hydrogen and nitrogen (<0.1 wt%) are detectable according to the microanalysis results (ESI, Table S1†) with a negligible amount of carbon (<0.5 wt%) in the $LiCoPO_4$ samples.

The electrochemical performance of $LiCoPO_4$ samples was assessed by galvanostatic cycling of Li half cells. The initial charge/discharge curves and the variations in discharge capacity and coulombic efficiency $\left(\text{calculated by } \frac{\text{discharge capacity}}{\text{charge capacity}} \times 100\% \text{ at each cycle}\right)$ over the first 40 cycles of $LiCoPO_4$ fired in Ar, air, 5% H_2/N_2 and NH_3

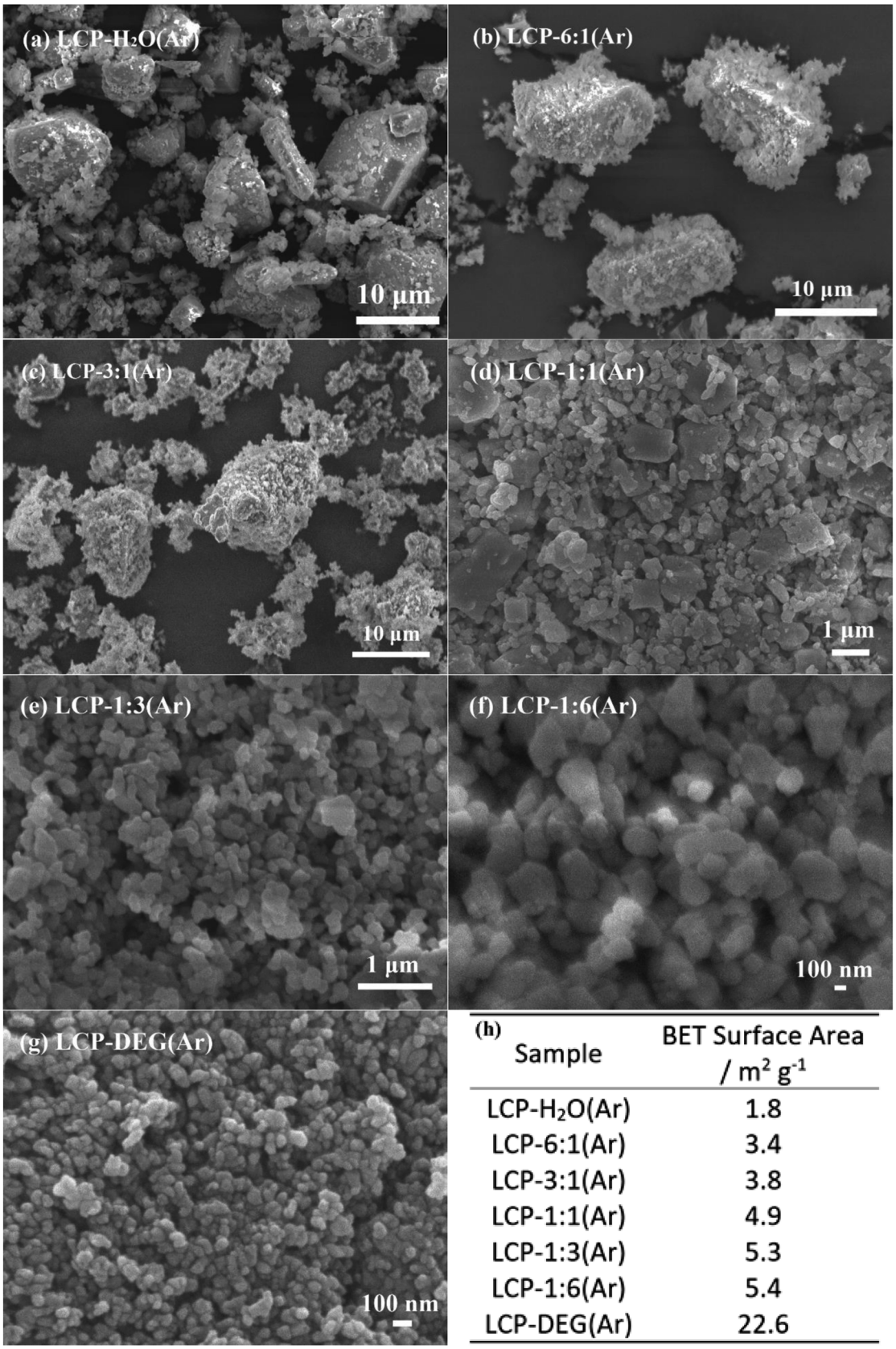

(h)

Sample	BET Surface Area / $m^2 g^{-1}$
LCP-H_2O(Ar)	1.8
LCP-6:1(Ar)	3.4
LCP-3:1(Ar)	3.8
LCP-1:1(Ar)	4.9
LCP-1:3(Ar)	5.3
LCP-1:6(Ar)	5.4
LCP-DEG(Ar)	22.6

Fig. 1 (a–g) SEM images of $LiCoPO_4$ samples synthesised by the solvothermal method, using H_2O/DEG solvent mixture with various volume ratios, followed by firing at 600 °C in Ar. (h) BET surface area of $LiCoPO_4$ samples.

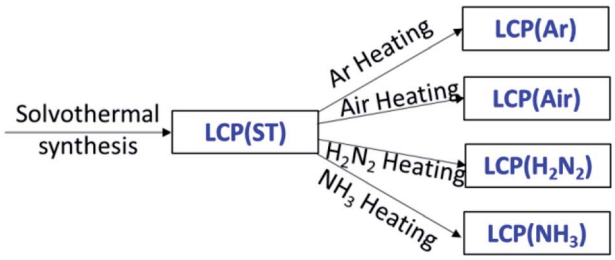

Scheme 1 Solvothermal synthesis to prepare $LiCoPO_4$, using 1 : 6 (v/v) H_2O/DEG co-solvent, followed by firing at 600 °C in Ar, air, 5% H_2/N_2 or NH_3.

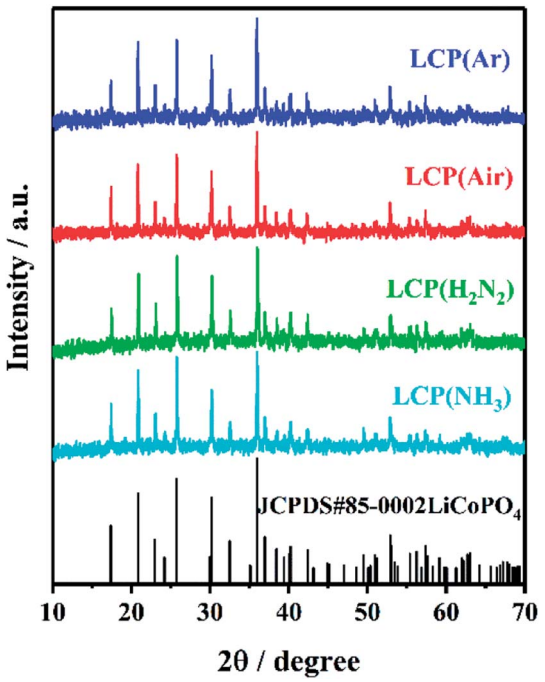

Fig. 2 XRD patterns of $LiCoPO_4$ samples heated under Ar, air, 5% H_2/N_2 and NH_3, respectively, at 600 °C (labels explained in Scheme 1). The black stick pattern denotes the literature positions and intensities of $LiCoPO_4$ reflections.[85]

are shown in Fig. 4. LCP(Ar), LCP(air), LCP(H_2N_2) and LCP(NH_3) had initial discharge capacities of 147, 130, 139 and 132 mA h g^{-1}, respectively. The capacity of LCP(Ar) decayed gradually with continuous cycling, retaining 102 mA h g^{-1} after 40 cycles, and 88 mA h g^{-1} after 57 cycles. The low coulombic efficiency values in the first cycle for these samples are caused by the decomposition of the electrolyte during charge at high potentials.[62,86] The coulombic efficiency of LCP(Ar), which improved upon cycling, was 92% in the second cycle and maintains values higher than 95% after five cycles. $LiCoPO_4$ fired in air or in reducing gases had lower initial discharge capacities and lost capacity more rapidly on cycling. A comparison of relevant articles using a hydrothermal/solvothermal methodology in the synthesis of $LiCoPO_4$ olivine phosphate cathodes is presented in Table 1. The obtained specific capacity and cycle stability of uncoated LCP(Ar) in our case is comparable or higher than most previous studies, even though in most of these reports $LiCoPO_4$ has been optimised with conductive coatings (*e.g.* carbon). Overall the results suggested that Ar firing was the most effective heat treatment to apply for the crystallisation of $LiCoPO_4$, but since air firing is also common in this system,[75,87–89] both samples as well as uncrystallised $LiCoPO_4$ were carried forward to test the surface modification of $LiCoPO_4$ with TiN, RuO_2 and carbon.

Synthesis, microstructure and electrochemistry of $LiCoPO_4$ modified with TiN, RuO_2 or C

Three kinds of $LiCoPO_4$ were chosen for coating, the uncrystallised $LiCoPO_4$ directly after solvothermal synthesis, with the advantage of a single heating step, and the $LiCoPO_4$ already crystallised in Ar or air (Scheme 2). RuO_2 and C coatings were prepared by manually grinding the precursors ($RuCl_3 \cdot xH_2O$ or sucrose) together with $LiCoPO_4$, then firing under Ar.[45,57] This solid-state process proved to be an easy and effective method to achieve carbon coatings on $LiCoPO_4$.[25,45] TiN coating used a propylamine-crosslinked sol–gel method, then firing under Ar or NH_3. This sol–gel process has been shown to be effective to achieve TiN coatings onto LIB cathode materials according to our previous research.[53] Scheme 2 summarises these approaches.

All the X-ray diffraction peaks of the resulting TiN, RuO_2 and C coated $LiCoPO_4$ samples (Fig. 5) can be indexed to the standard olivine $LiCoPO_4$ structure. The characteristic peaks of TiN and RuO_2 were not detectable in coated $LiCoPO_4$ composites due to their low concentrations. Carbon coatings on battery materials are typically amorphous when heating at around 600 °C,[48,61,81] and also were not visible in the diffraction data. Fig. S4–S6† show the Rietveld fits to the XRD data, which yielded typical $LiCoPO_4$ lattice parameters (ESI, Tables S2–S4†),[84] suggesting that the coating processes did not affect the crystal structure of $LiCoPO_4$.

Fig. 6 shows the initial charge/discharge curves at 0.1C and the cycle stability of electrodes produced from the coated materials. Carbon is the most commonly used battery material coating, but RuO_2 has been used to coat electroactive materials to offer a high electronic conductivity and quick Li permeation.[95–98] Due to its good electrical conductivity, chemical stability and thermal stability, TiN has been combined with other electrode materials to form structured composites with improved conductivity and stability.[53,55,56]

RuO_2 coating of the unfired $LiCoPO_4$ (Fig. 6a and b) resulted in a higher initial discharge capacity of 148 mA h g^{-1} as expected due to the utility of RuO_2 in generating very effective mixed conducting heterogeneous electrodes.[57] However, its capacity drops quickly in subsequent cycles. The carbon coated samples had lower capacities than their uncoated counterparts, and the drop in capacity when C content was increased from 5% to 10% suggests that the thicker carbon coating hindered lithium diffusion.

Air fired $LiCoPO_4$ samples coated with TiN, RuO_2, 5 wt% C or 10 wt% C (Fig. 6c and d) had initial discharge capacities of 130,

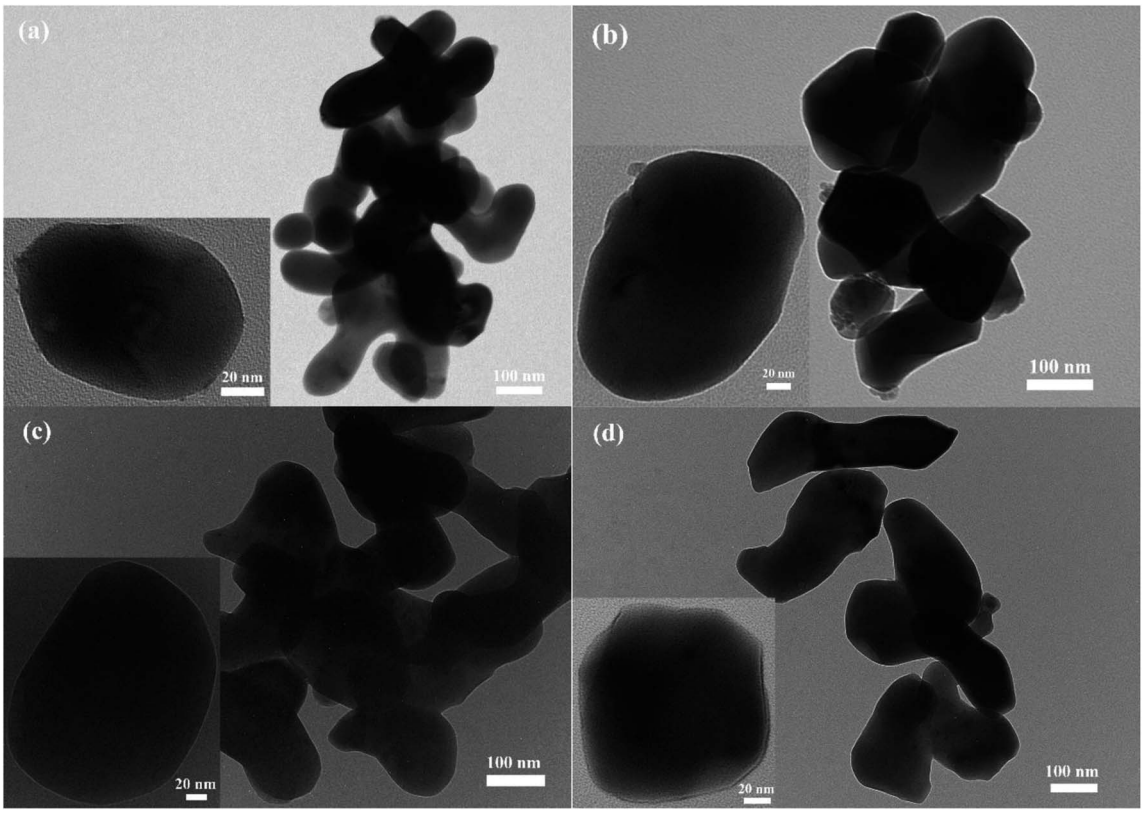

Fig. 3 TEM images of (a) LCP(Ar), (b) LCP(air), (c) LCP(H_2N_2) and (d) LCP(NH_3) (scale bar = 100 nm). (Inset) magnified TEM images of single $LiCoPO_4$ particle (scale bar = 20 nm). Sample labels are explained in Scheme 1.

144, 145 and 139 mA h g^{-1}, respectively. The TiN coated sample retained a fairly large fraction of the initial capacity during continuous cycling.[53] However, the cycle stability was quite similar to the uncoated LCP(air) (Fig. 4), so the coatings did not significantly improve the electrochemical performance of $LiCoPO_4$. Notably cycle stability was less good with RuO_2 or C coatings than with uncoated material.

A similar position was observed with the Ar-fired $LiCoPO_4$ (Fig. 6e and f). The capacities of the C or TiN coated samples dropped to around 100 mA h g^{-1} over 10 cycles, a poorer cycle stability than that of the uncoated LCP(Ar), which retained 102 mA h g^{-1} after 40 cycles (Fig. 4). The coatings did not deliver the expected improvement in electrochemical performance of $LiCoPO_4$. However, the purpose of the conductive agent coating

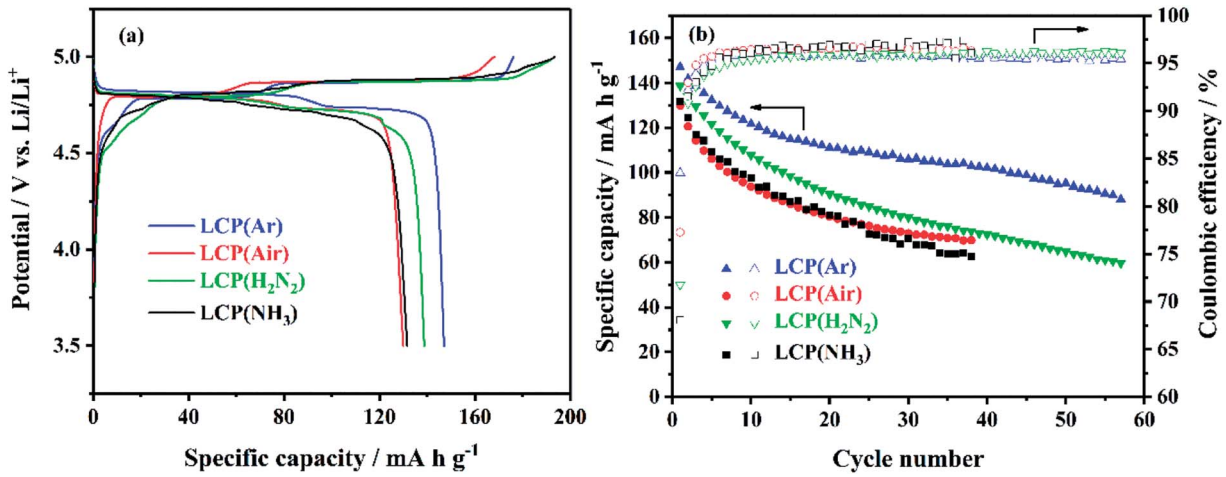

Fig. 4 (a) The initial cycle voltage profile *vs.* specific capacity and (b) specific capacity and coulombic efficiency *vs.* cycle number of $LiCoPO_4$/Li half cells under galvanostatic cycling between 3.5 and 5 V at 0.1C (sample labels explained in Scheme 1).

Table 1 Morphologies and electrochemical behaviours of $LiCoPO_4$ samples synthesised under hydrothermal/solvothermal conditions (shown in chronological order with the most recent study first)

Morphology, particle size	Rate performance, mA h g^{-1}	Cycle stability	Ref.
Nanoparticles, 150 nm	147 (0.1C)	102 mA h g^{-1} at 0.1C after 40 cycles	This work
Irregular nanoparticle	160 (0.1C), 138 (1C), 120 (2C), 88 (5C)	138 mA h g^{-1} at 0.1C after 100 cycles	73
Hexagonal platelets, 200 × 100 × 50 nm to 1.2 × 1.2 × 0.5 μm	136 (0.1C), 125 (0.2C), 115 (0.5C), 105 (1C), 95 (2C)	108 mA h g^{-1} at 0.5C after 15 cycles	63
Square, rhombic and hexagonal platelets, 600–800 × 400–600 × 100–150 nm to 9 × 7 × 3 μm	141 (0.1C), 135 (0.2C), 130 (0.5C), 123 (1C), 112 (2C)	125 mA h g^{-1} at 0.5C after 15 cycles	44
Spherical or oblong spheroid, 50–250 nm	145 (0.1C)	74 mA h g^{-1} at 0.1C after 20 cycles	90
Irregular particles, 390 nm to 2.8 μm	135 (0.1C), 132 (0.5C), 125 (1C), 117 (2C), 101 (5C)	70 mA h g^{-1} 0.1C after 30 cycles	42
Irregular particles, 200 nm to 1 μm	155 (0.1C), 129 (1C), 98 (5C), 70 (10C), 51 (20C)	141 mA h g^{-1} at 0.1C after 80 cycles	74
Particles, 100–500 nm	97 (0.1C)	82 mA h g^{-1} at 0.1C after 20 cycles	85
Particles, 500 nm to 10 μm	124 (0.1C), 111 (0.5C), 100 (1C), 85 (2C), 51 (5C)	103 mA h g^{-1} at 0.1C after 100 cycles	45
Hexagonal platelets, 400–600 × 700–800 × 100–220 nm	137 (0.1C), 114 (0.5C), 97 (2C)	78 mA h g^{-1} at 0.5C after 100 cycles	62
Hexagonal platelets, thickness < 200 nm	120 (0.1C), 85 (0.5C), 75 (1C)	90 mA h g^{-1} at 0.1C after 10 cycles	64
Flower-like, 5–10 μm (compose of plate-like, 1–2 μm × 200 nm)	107 (0.05C), 60 (2C)	30 mA h g^{-1} at 0.05C after 20 cycles	78
Hexagonal/octagonal platelet, thickness of 50–100 nm	95 (0.1C), 76 (0.5C)	75 mA h g^{-1} at 0.1C after 10 cycles	91 and 92
Nanoparticles agglomeration, 2–3 μm	105 (0.2C)	95 mA h g^{-1} at 0.2C after 30 cycles	93
Hedgehog-like, 5–8 μm (compose of nanorods, 40 nm × 1 μm)	136 (0.1C), 85 (5C)	124 mA h g^{-1} at 0.1C after 50 cycles	94
Rod, 300–700 nm × 5 μm	65 (0.1C)	50 mA h g^{-1} at 0.1C after 10 cycles	77
Cubes, 1.2–1.5 μm × 250 nm	52 (0.1C)	15 mA h g^{-1} at 0.1C after 25 cycles	76

was to create a conductive network among the $LiCoPO_4$ particles to improve the conductivity of the composites. These results show that, using these optimised solvothermal conditions, the conductivity of the bare LCP(Ar) sample is good enough to provide competitive specific capacity and cycle stability.

Further investigation of $LiCoPO_4$ fired in Ar and air

The electronic and ionic conductivity of $LiCoPO_4$ powders fired in Ar and air was evaluated with current–voltage measurements and electrochemical impedance spectroscopy. $LiCoPO_4$ samples were pressed, sintered and gold-coated to produce self-standing $LiCoPO_4$ disks, which were dry contacted with two silver paste electrodes. The linear current–voltage plots (Fig. 7) showed that the LCP(Ar) pellet behaves as a resistor and the current–voltage relationship is given by Ohm's law: $V = IR$. Hence, the resistance of the $LiCoPO_4$ samples can be estimated as being equal to the inverse of the slope of the current–voltage plot. The conductivity of the samples is given by $\sigma = \frac{1}{R}\frac{l}{A}$, where σ is the conductivity, l is the thickness of the $LiCoPO_4$ pellets (0.48 mm for LCP(Ar) and 0.64 mm for LCP(air) sample), A is the area of the $LiCoPO_4$ pellets (95 mm^2), and R is the resistance (42.2 Ω for LCP(Ar) and 1.7×10^7 Ω for LCP(air) sample). The conductivities of LCP(Ar) and LCP(air) are calculated to be $\sim 10^{-3}$ S cm^{-1} and $\sim 10^{-9}$ S cm^{-1}, respectively. Current–voltage plots with larger voltage ranges are shown in Fig. S7,† and they are in agreement with those in Fig. 7.

These conductivity results can be confirmed by electrochemical impedance spectroscopy measurements of the gold-coated pressed $LiCoPO_4$ pellets, as presented in Fig. S8.† The impedance of the LCP(Ar) sample shows purely resistor behaviour (ESI, Fig. S8a†). This is in agreement with the fact that this sample has reasonably high electronic conductivity of $\sim 10^{-3}$ S cm^{-1}, estimated from the value of the resistance and taking into account the dimension of the pellet. On the other hand, the LCP(air) sample shows much higher values of impedance (ESI, Fig. S8b†). This is ascribed to the fact that this sample has much higher electronic resistance, thus it behaves as a resistor coupled to a capacitor (or a constant phase element) in parallel. In addition, the surface of the pellet cannot be polished prior to gold coating (due to the fragility of the pellet), thus the $LiCoPO_4$–gold interphase behaves as a Warburg element, rather than a capacitor or a constant phase element. By fitting the data to the equivalent circuit shown in Fig. S8b,† the electronic conductivity of the LCP(air) sample is estimated to $\sim 10^{-9}$ S cm^{-1}. This is in agreement with the estimation of the total conductivity of the samples by using current–voltage measurements, and the dramatic difference in conductivity

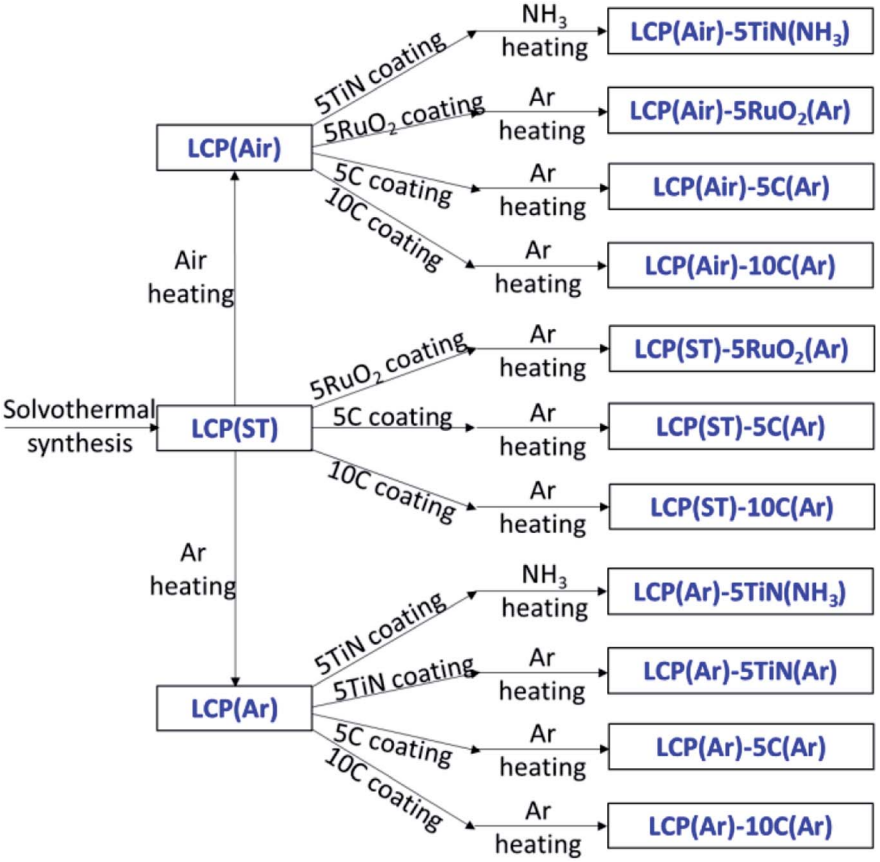

Scheme 2 Preparation conditions and sample labels for TiN, RuO_2 or C coated $LiCoPO_4$ materials.

between these two samples explains the fact that the sample fired in Ar showed better specific capacity and cycling performance.

Wolfenstine *et al.* investigated the effect of added carbon on the electronic conductivity and specific capacity of $LiCoPO_4$, and found that the added carbon was partly consumed to

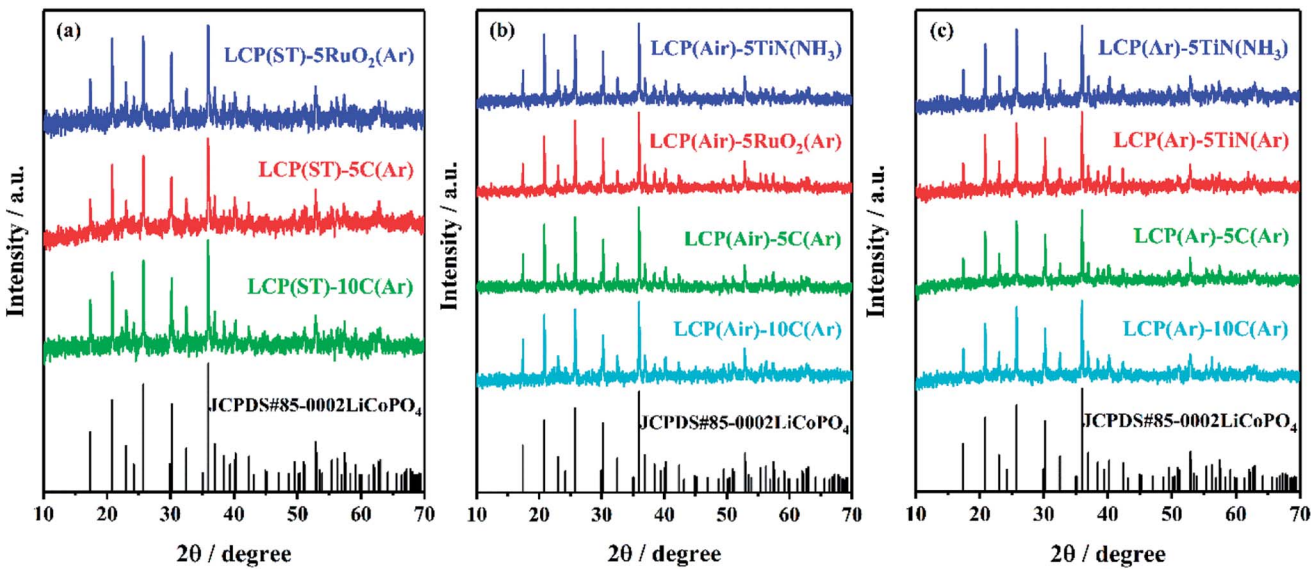

Fig. 5 XRD patterns of uncrystallised $LiCoPO_4$ directly after solvothermal synthesis (left), and $LiCoPO_4$ heated under air (centre) or Ar (right) at 600 °C, then modified with TiN, RuO_2 and carbon, respectively (labels explained in Scheme 2). The black stick pattern denotes the literature positions and intensities of $LiCoPO_4$ reflections.[85]

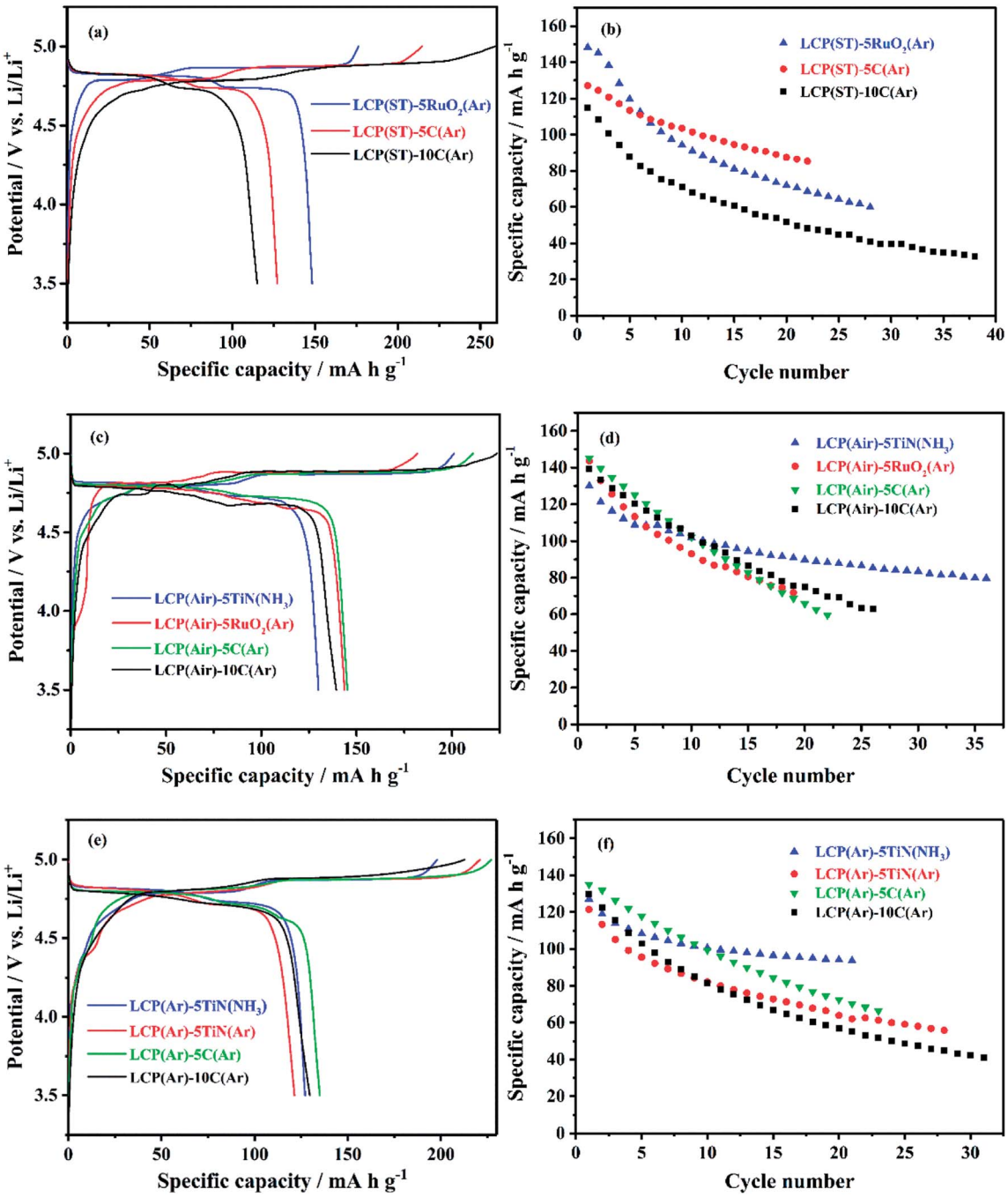

Fig. 6 (a), (c) and (e) The initial cycle voltage profile *vs.* specific capacity, and (b), (d) and (f) specific capacity *vs.* cycle number of TiN, RuO_2 or C coated $LiCoPO_4$ samples made into Li half cells, under galvanostatic cycling between 3.5 and 5 V at 0.1C (sample labels explained in Scheme 2, with the percentage of TiN, RuO_2 or C in the composite written after the hyphen).

reduce the $LiCoPO_4$ surface layers to Co_2P during heating under Ar atmosphere.[33,34] The formation of highly conductive ($\sim 10^{-1}$ S cm^{-1}) Co_2P phase in $LiCoPO_4$ cathode led to improved electrochemical performance. As the amount of the Co_2P phase increased to 4 wt%, the electronic conductivity increased to $\sim 10^{-4}$ S cm^{-1} with a maximum discharge capacity of $\sim$120 mA h g^{-1} obtained. However, for $LiCoPO_4$ cathodes with higher concentrations of Co_2P, the capacities dropped rapidly due to the electrochemically inert Co_2P phase, which improves the electronic conductivity but tends to hinder the Li^+ insertion/extraction. Similar phenomena were also observed by Xu[99] and Indris *et al.*[88] Ma *et al.* demonstrated that the presence of Co_2P can accelerate the electrolyte decomposition at high voltage in the charge process for $LiCoPO_4$ due to the catalytic property of Co_2P.[100] Dimesso *et al.* suggested that the formation of Co_2P occurs due to reduction reactions at the grain boundaries of the $LiCoPO_4$ crystalline phase during annealing at high temperatures.[101–107] Brutti *et al.* synthesized $LiCoPO_4$ *via* a solvothermal

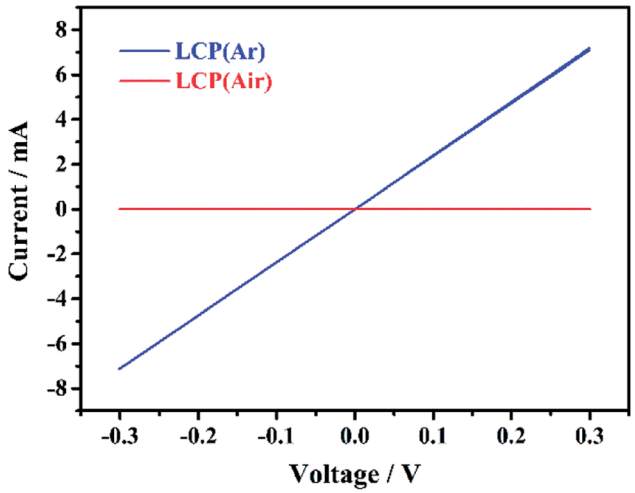

Fig. 7 Current–voltage plots (3 cycles each) for $LiCoPO_4$ samples fired in Ar and air, respectively, cycling at scanning rate of 20 mV s^{-1}, showing the ohmic behaviour of the samples (labels explained in Scheme 1).

synthesis followed by heating under Ar atmosphere. It was found that the heating promotes Co_2P precipitation on the $LiCoPO_4$ particles surface together with loss of organic by-products formed in the solvothermal synthesis.[108] Nallathamby *et al.* confirmed that the presence of Co_2P as a second phase enhanced the conductivity and electrochemical performance of $LiCoPO_4$. It was found that the Co_2P is achievable only in an inert atmosphere. The $LiCoPO_4$ cathode showed a discharge capacity of 123 mA h g^{-1} at 0.1C with capacity retention of 89% after 30 cycles, and rate capability of 81 mA h g^{-1} at 5C.[61]

Based on the discussion above, the better conductivity of $LiCoPO_4$ heated in Ar was considered likely to be due to the presence of Co_2P on the surface on $LiCoPO_4$. X-ray photoelectron spectroscopy (XPS) of $LiCoPO_4$ samples fired under Ar and air is shown in Fig. 8. These two samples had similar Li 1s and C 1s spectra (ESI, Fig. S9†). Particularly, for the $LiCoPO_4$ fired under Ar, the Li 1s signal located at 55.7 eV is well in accordance with the value reported for $LiCoPO_4$.[61] The C 1s spectrum consists of three peaks, with the main component at 285.0 eV corresponding to C–C, and the other two peaks observed at 287.1 eV and 289.0 eV attributed to C–O and O=C–O environments of carbon.[109] Fig. 8 shows clear differences between the chemical environments present in the P 2p and O 1s spectra of these samples. For the $LiCoPO_4$ fired under Ar, the O 1s spectrum with a binding energy of 531.6 eV is in agreement with the air-fired sample and with the $(PO_4)^{3-}$ environment in $LiCoPO_4$,[61] but an additional weak peak at 529.1 eV demonstrates the presence of a small amount of metal oxide (*e.g.* Li_2O with binding energy of 528.6 eV for O 1s spectrum).[110–112] The P 2p spectrum ($2p_{3/2}$ and $2p_{1/2}$ doublet) shows the main component at 133.5–134.4 eV in accordance with $LiCoPO_4$,[91] and a doublet at lower binding energy (130.9–131.8 eV) that corresponds to Co_2P.[113] A small shift in binding energy of P 2p in Co_2P (expected at around 129 eV) is likely to be due to a differential charging effect resulting from the different electrical conductivities at the surfaces of $LiCoPO_4$ and Co_2P.[113–115] Co_2P formation in Ar fired $LiCoPO_4$ is attributed to the carbon-containing organic solvent (DEG) chosen for the synthesis,

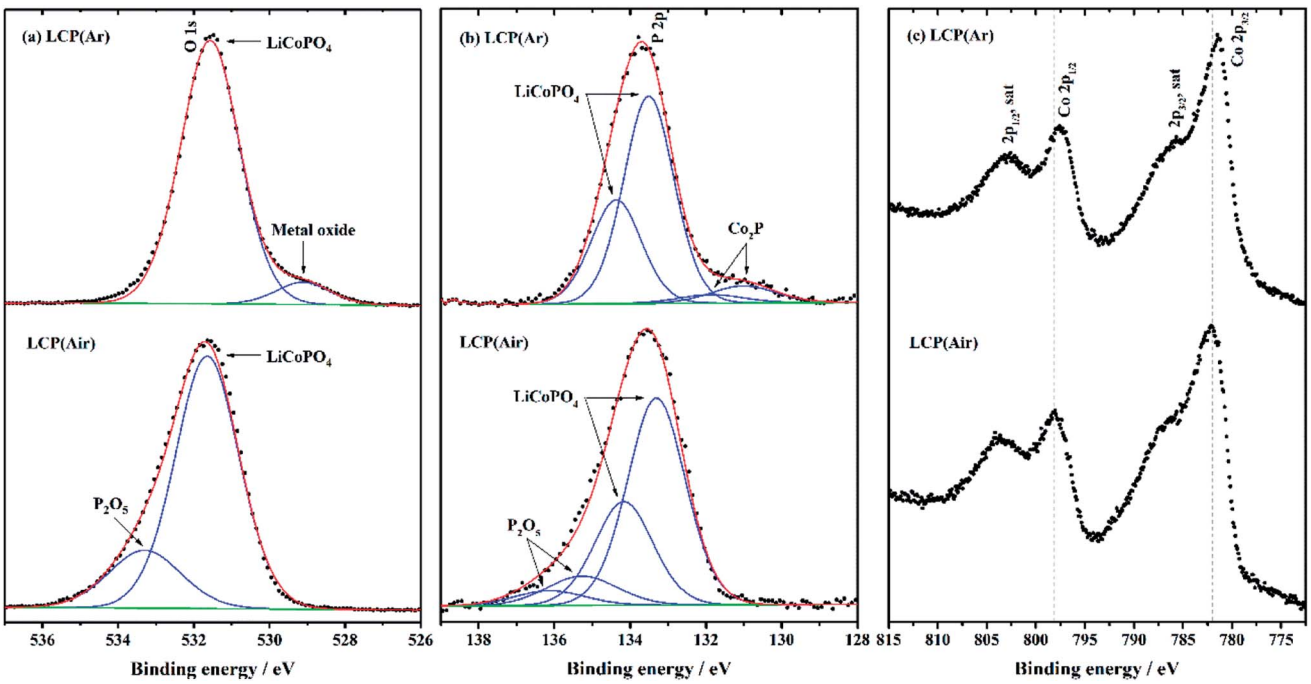

Fig. 8 P 2p, O 1s and Co 2p XPS spectra of $LiCoPO_4$ samples fired in Ar and air, respectively (labels explained in Scheme 1). The data points and enveloped fitting plot are overlaid in black dots and a red line, respectively. The fitting peaks and background are shown in blue and green, respectively.

which can decompose at high temperature and the resulting carbon can cause carbothermal reduction to reduce the $LiCoPO_4$ surface layers to Co_2P during heating under inert atmosphere.[33,34,61,101,105,108] This process also explains the relatively low carbon content measured in these samples by microanalysis. The Co 2p spectra are not fitted due to the complexity of the 2p spectra resulting from peak asymmetries, complex doublet splitting, shake-up and plasmon loss structure, and uncertain, overlapping binding energies.[116] For the $LiCoPO_4$ fired under Ar, the $2p_{3/2}$ and $2p_{1/2}$ doublet in the Co 2p spectrum has binding energy values of 781.5 and 797.6 eV, respectively. In LCP(air) these peaks are observed at 782.1 eV and 798.1 eV ($2p_{3/2}$ and $2p_{1/2}$). The shift to lower binding energy can be attributed to the presence of Co_2P in LCP(Ar).[113] The difference of binding energy between Co $2p_{3/2}$ and its satellite peak is in agreement with the Co^{2+} environment in $LiCoPO_4$.[91,116] For the $LiCoPO_4$ fired under air, a new chemical environment corresponding to P_2O_5 is identified with additional peaks in the P 2p (135.3–136.1 eV) and O 1s (533.3 eV) spectra.[117,118]

The best specific capacity (147 mA h g^{-1}) and cycling performance of $LiCoPO_4$ shown in Fig. 4, achieved by heating in Ar, can be attributed the good electronic conductivity ($\sim 10^{-3}$ S cm^{-1}) of $LiCoPO_4$ due to the presence of Co_2P after firing under Ar. Also, the nanosized $LiCoPO_4$ obtained from DEG promoted solvothermal synthesis provides short Li-ion migration paths, and facilitates easier Li-ion transfer within the material. The $LiCoPO_4$ fired in air showed relatively low initial specific capacity of 130 mA h g^{-1}. This could be attributed to the poor electric conductivity of $\sim 10^{-9}$ S cm^{-1} (Fig. 7 and S8†) as there is no evidence of the presence of Co_2P in this sample.

Conclusions

A facile solvothermal synthesis to prepare olivine-structured $LiCoPO_4$ for high-voltage cathodes in LIBs has been developed, using various ratios of water/diethylene glycol as solvent, followed by thermal treatment under Ar, air, 5% $H_2 + N_2$ or NH_3. The diethylene glycol plays an important role in tailoring the particle size of $LiCoPO_4$. It is found that using a ratio of water/diethylene glycol of 1 : 6 (v/v), $LiCoPO_4$ is obtained with a homogenous particle size of $\sim$150 nm. The $LiCoPO_4$ prepared after heating in Ar exhibits high initial discharge capacity of 147 mA h g^{-1} at 0.1C with capacity retention of 70% after 40 cycles. This is attributed to the enhanced electronic conductivity of $LiCoPO_4$ due to the presence of Co_2P after firing under Ar. The specific capacity and cycle stability of carbon, TiN and RuO_2 coated $LiCoPO_4$ were also examined, but did not improve the performance of the material. Hence, under our solvothermal synthesis conditions, $LiCoPO_4$ with good discharge capacity and cycle stability, without need for separate conductivity coatings, were produced.

Conflicts of interest

There are no conflicts of interest to declare.

Acknowledgements

MZ thanks the China Scholarship Council (CSC) and the University of Southampton for support. NGA thanks the EPSRC for an early career fellowship (EP/N024303/1) and SS is supported by EPSRC under EP/N035437/1. All data supporting this study are openly available from the University of Southampton repository at https://doi.org/10.5258/SOTON/D0767.

Notes and references

1 P. Poizot and F. Dolhem, *Energy Environ. Sci.*, 2011, **4**, 2003–2019.
2 J. P. Correa-Baena, M. Saliba, T. Buonassisi, M. Grätzel, A. Abate, W. Tress and A. Hagfeldt, *Science*, 2017, **358**, 739–744.
3 Z. M. Bhat, R. Thimmappa, M. C. Devendrachari, A. R. Kottaichamy, S. P. Shafi, S. Varhade, M. Gautam and M. O. Thotiyl, *J. Phys. Chem. Lett.*, 2018, **9**, 388–392.
4 M. Guo, W. Song and J. Buhain, *Renewable Sustainable Energy Rev.*, 2015, **42**, 712–725.
5 L. Dimesso, C. Forster, W. Jaegermann, J. P. Khanderi, H. Tempel, A. Popp, J. Engstler, J. J. Schneider, A. Sarapulova, D. Mikhailova, L. A. Schmitt, S. Oswald and H. Ehrenberg, *Chem. Soc. Rev.*, 2012, **41**, 5068–5080.
6 N. Mahne, S. E. Renfrew, B. D. McCloskey and S. A. Freunberger, *Angew. Chem., Int. Ed.*, 2018, **57**, 5529–5533.
7 E. Mourad, L. Coustan, P. Lannelongue, D. Zigah, A. Mehdi, A. Vioux, S. A. Freunberger, F. Favier and O. Fontaine, *Nat. Mater.*, 2017, **16**, 446–453.
8 N. C. Dargily, R. Thimmappa, Z. M. Bhat, M. C. Devendrachari, A. R. Kottaichamy, M. Gautam, S. P. Shafi and M. O. Thotiyl, *J. Phys. Chem. Lett.*, 2018, **9**, 2492–2497.
9 N. Dupre, M. Cuisinier, J. F. Martin and D. Guyomard, *ChemPhysChem*, 2014, **15**, 1922–1938.
10 F. Yu, L. Zhang, Y. Li, Y. An, M. Zhu and B. Dai, *RSC Adv.*, 2014, **4**, 54576–54602.
11 S. Deng, H. Wang, H. Liu, J. Liu and H. Yan, *Nano-Micro Lett.*, 2014, **6**, 209–226.
12 L.-X. Yuan, Z.-H. Wang, W.-X. Zhang, X.-L. Hu, J.-T. Chen, Y.-H. Huang and J. B. Goodenough, *Energy Environ. Sci.*, 2011, **4**, 269–284.
13 C. Gong, Z. Xue, S. Wen, Y. Ye and X. Xie, *J. Power Sources*, 2016, **318**, 93–112.
14 T. V. S. L. Satyavani, A. Srinivas Kumar and P. S. V. Subba Rao, *Engineering Science and Technology, an International Journal*, 2016, **19**, 178–188.
15 H. Wu, Q. Liu and S. Guo, *Nano-Micro Lett.*, 2014, **6**, 316–326.
16 A. Eftekhari, *J. Power Sources*, 2017, **343**, 395–411.
17 J. Wang and X. Sun, *Energy Environ. Sci.*, 2012, **5**, 5163–5185.
18 Y. Wang, P. He and H. Zhou, *Energy Environ. Sci.*, 2011, **4**, 805–817.
19 Z. Yang, Y. Dai, S. Wang and J. Yu, *J. Mater. Chem. A*, 2016, **4**, 18210–18222.

20 J. Wang and X. Sun, *Energy Environ. Sci.*, 2015, **8**, 1110–1138.
21 Z. Bi, X. Zhang, W. He, D. Min and W. Zhang, *RSC Adv.*, 2013, **3**, 19744–19751.
22 W.-J. Zhang, *J. Power Sources*, 2011, **196**, 2962–2970.
23 D. Jugović and D. Uskoković, *J. Power Sources*, 2009, **190**, 538–544.
24 G. K. Singh, G. Ceder and M. Z. Bazant, *Electrochim. Acta*, 2008, **53**, 7599–7613.
25 M. Zhang, N. Garcia-Araez and A. L. Hector, *J. Mater. Chem. A*, 2018, **6**, 14483–14517.
26 A. Mauger, C. M. Julien, M. Armand, J. B. Goodenough and K. Zaghib, *Curr. Opin. Electrochem.*, 2017, **6**, 63–69.
27 J. Ludwig and T. Nilges, *J. Power Sources*, 2018, **382**, 101–115.
28 M. Hu, X. L. Pang and Z. Zhou, *J. Power Sources*, 2013, **237**, 229–242.
29 L. Fang, H. J. Zhang, Y. Zhang, L. Liu and Y. Wang, *J. Power Sources*, 2016, **312**, 101–108.
30 A. Örnek, *J. Power Sources*, 2017, **356**, 1–11.
31 J. Wolfenstine, U. Lee, B. Poese and J. L. Allen, *J. Power Sources*, 2005, **144**, 226–230.
32 K. Tadanaga, F. Mizuno, A. Hayashi, T. Minami and M. Tatsumisago, *Electrochemistry*, 2003, **71**, 1192–1195.
33 J. Wolfenstine, *J. Power Sources*, 2006, **158**, 1431–1435.
34 J. Wolfenstine, J. Read and J. L. Allen, *J. Power Sources*, 2007, **163**, 1070–1073.
35 J. L. Allen, T. Thompson, J. Sakamoto, C. R. Becker, T. R. Jow and J. Wolfenstine, *J. Power Sources*, 2014, **254**, 204–208.
36 K. Rissouli, K. Benkhouja, J. Ramos-Barrado and C. Julien, *Mater. Sci. Eng., B*, 2003, **98**, 185–189.
37 M. Prabu, S. Selvasekarapandian, M. V. Reddy and B. V. R. Chowdari, *J. Solid State Electrochem.*, 2012, **16**, 1833–1839.
38 J. Xie, N. Imanishi, T. Zhang, A. Hirano, Y. Takeda and Y. Yamamoto, *J. Power Sources*, 2009, **192**, 689–692.
39 M. Prabu, S. Selvasekarapandian, A. R. Kulkarni, S. Karthikeyan, G. Hirankumar and C. Sanjeeviraja, *Solid State Sci.*, 2011, **13**, 1714–1718.
40 D. Shanmukaraj and R. Murugan, *Ionics*, 2004, **10**, 88–92.
41 D. Morgan, A. Van der Ven and G. Ceder, *Electrochem. Solid-State Lett.*, 2004, **7**, A30–A32.
42 Y. Maeyoshi, S. Miyamoto, Y. Noda, H. Munakata and K. Kanamura, *J. Power Sources*, 2017, **337**, 92–99.
43 Y. H. Ikuhara, X. Gao, C. A. J. Fisher, A. Kuwabara, H. Moriwake, K. Kohama, H. Iba and Y. Ikuhara, *J. Mater. Chem. A*, 2017, **5**, 9329–9338.
44 J. Ludwig, C. Marino, D. Haering, C. Stinner, H. A. Gasteiger and T. Nilges, *J. Power Sources*, 2017, **342**, 214–223.
45 B. R. Wu, H. L. Xu, D. B. Mu, L. L. Shi, B. Jiang, L. Gai, L. Wang, Q. Liu, L. B. Ben and F. Wu, *J. Power Sources*, 2016, **304**, 181–188.
46 N. Laszczynski, A. Birrozzi, K. Maranski, M. Copley, M. E. Schuster and S. Passerini, *J. Mater. Chem. A*, 2016, **4**, 17121–17128.
47 S. Brutti, J. Manzi, D. Meggiolaro, F. M. Vitucci, F. Trequattrini, A. Paolone and O. Palumbo, *J. Mater. Chem. A*, 2017, **5**, 14020–14030.
48 Y. Liu, M. Zhang, Y. Li, Y. Hu, M. Zhu, H. Jin and W. Li, *Electrochim. Acta*, 2015, **176**, 689–693.
49 B. León, C. P. Vicente, J. Tirado, P. Biensan and C. Tessier, *J. Electrochem. Soc.*, 2008, **155**, A211–A216.
50 H. Liu, G. X. Wang, D. Wexler, J. Z. Wang and H. K. Liu, *Electrochem. Commun.*, 2008, **10**, 165–169.
51 Y. Liu, C. Mi, C. Yuan and X. Zhang, *J. Electroanal. Chem.*, 2009, **628**, 73–80.
52 Y.-D. Li, S.-X. Zhao, C.-W. Nan and B.-H. Li, *J. Alloys Compd.*, 2011, **509**, 957–960.
53 M. Zhang, N. Garcia-Araez, A. L. Hector and J. R. Owen, *J. Mater. Chem. A*, 2017, **5**, 2251–2260.
54 S. Dong, X. Chen, L. Gu, X. Zhou, L. Li, Z. Liu, P. Han, H. Xu, J. Yao, H. Wang, X. Zhang, C. Shang, G. Cui and L. Chen, *Energy Environ. Sci.*, 2011, **4**, 3502–3508.
55 I.-S. Kim, P. N. Kumta and G. E. Blomgren, *Electrochem. Solid-State Lett.*, 2000, **3**, 493–496.
56 M. Q. Snyder, S. A. Trebukhova, B. Ravdel, M. C. Wheeler, J. DiCarlo, C. P. Tripp and W. J. DeSisto, *J. Power Sources*, 2007, **165**, 379–385.
57 Y. S. Hu, Y. G. Guo, R. Dominko, M. Gaberscek, J. Jamnik and J. Maier, *Adv. Mater.*, 2007, **19**, 1963–1966.
58 L. Dimesso, C. Spanheimer and W. Jaegermann, *J. Power Sources*, 2013, **243**, 668–675.
59 T. Fukutsuka, T. Nakagawa, K. Miyazaki and T. Abe, *J. Power Sources*, 2016, **306**, 753–757.
60 I. C. Jang, C. G. Son, S. M. G. Yang, J. W. Lee, A. R. Cho, V. Aravindan, G. J. Park, K. S. Kang, W. S. Kim, W. I. Cho and Y. S. Lee, *J. Mater. Chem.*, 2011, **21**, 6510–6514.
61 Gangulibabu, K. Nallathamby, D. Meyrick and M. Minakshi, *Electrochim. Acta*, 2013, **101**, 18–26.
62 J. Ludwig, C. Marino, D. Haering, C. Stinner, D. Nordlund, M. M. Doeff, H. A. Gasteiger and T. Nilges, *RSC Adv.*, 2016, **6**, 82984–82994.
63 J. Ludwig, D. Haering, M. M. Doeff and T. Nilges, *Solid State Sci.*, 2017, **65**, 100–109.
64 J. Manzi, M. Curcio and S. Brutti, *Nanomaterials*, 2015, **5**, 2212–2230.
65 M. G. Palmer, J. T. Frith, A. L. Hector, A. W. Lodge, J. R. Owen, C. Nicklin and J. Rawle, *Chem. Commun.*, 2016, **52**, 14169–14172.
66 B. M. Gray, S. Hassan, A. L. Hector, A. Kalaji and B. Mazumder, *Chem. Mater.*, 2009, **21**, 4210–4215.
67 A. W. Jackson and A. L. Hector, *J. Mater. Chem.*, 2007, **17**, 1016–1022.
68 A. L. Hector, *Chem. Soc. Rev.*, 2007, **36**, 1745–1753.
69 A. Larson, R. Von Dreele, L. Finger, M. Kroeker and B. Toby, *J. Appl. Crystallogr.*, 2001, **34**, 210–213.
70 D. A. Shirley, *Phys. Rev. B*, 1972, **5**, 4709–4714.
71 G. Wang, S. Bewlay, K. Konstantinov, H. Liu, S. Dou and J.-H. Ahn, *Electrochim. Acta*, 2004, **50**, 443–447.
72 S. Shi, L. Liu, C. Ouyang, D.-S. Wang, Z. Wang, L. Chen and X. Huang, *Phys. Rev. B*, 2003, **68**, 195108–195112.
73 A. Örnek, *J. Alloys Compd.*, 2017, **710**, 809–818.

74 A. Örnek, A. Yesildag, M. Can and S. Akturk, *Mater. Res. Bull.*, 2016, **83**, 1–11.
75 R. Hanafusa, Y. Oka and T. Nakamura, *J. Electrochem. Soc.*, 2015, **162**, A3045–A3051.
76 A. V. Murugan, T. Muraliganth and A. Manthiram, *J. Electrochem. Soc.*, 2009, **156**, A79–A83.
77 Y. J. Zhao, S. J. Wang, C. S. Zhao and D. G. Xia, *Rare Met.*, 2009, **28**, 117–121.
78 C. Neef, H. P. Meyer and R. Klingeler, *Solid State Sci.*, 2015, **48**, 270–277.
79 J. Ludwig, D. Nordlund, M. M. Doeff and T. Nilges, *J. Solid State Chem.*, 2017, **248**, 9–17.
80 M. Türk, *J. Supercrit. Fluids*, 2000, **18**, 169–184.
81 H. H. Li, J. Jin, J. P. Wei, Z. Zhou and J. Yan, *Electrochem. Commun.*, 2009, **11**, 95–98.
82 T. N. L. Doan and I. Taniguchi, *J. Power Sources*, 2011, **196**, 5679–5684.
83 W. Hofmann and A. Schrader, *Arch. Eisenhuettenwes.*, 1936, **10**, 65–66.
84 S. Okada, S. Sawa, M. Egashira, J. Yamaki, M. Tabuchi, H. Kageyama, T. Konishi and A. Yoshino, *J. Power Sources*, 2001, **97**, 430–432.
85 K. J. Kreder, G. Assat and A. Manthiram, *Chem. Mater.*, 2016, **28**, 1847–1853.
86 N. N. Bramnik, K. Nikolowski, D. M. Trots and H. Ehrenberg, *Electrochem. Solid-State Lett.*, 2008, **11**, A89–A93.
87 H. H. Li, Y. P. Wang, X. L. Yang, L. Liu, L. Chen and J. P. Wei, *Solid State Ionics*, 2014, **255**, 84–88.
88 M. Kaus, I. Issac, R. Heinzmann, S. Doyle, S. Mangold, H. Hahn, V. S. K. Chakravadhanula, C. Kubel, H. Ehrenberg and S. Indris, *J. Phys. Chem. C*, 2014, **118**, 17279–17290.
89 V. Aravindan, Y. L. Cheah, W. C. Ling and S. Madhavi, *J. Electrochem. Soc.*, 2012, **159**, A1435–A1439.
90 K. J. Kreder and A. Manthiram, *ACS Energy Lett.*, 2017, **2**, 64–69.
91 S. Brutti, J. Manzi, A. De Bonis, D. Di Lecce, F. Vitucci, A. Paolone, F. Trequattrini and S. Panero, *Mater. Lett.*, 2015, **145**, 324–327.
92 S. Brutti, J. Manzi, A. De Bonis, D. Di Lecce, F. Vitucci, A. Paolone, F. Trequattrini and S. Panero, *Mater. Lett.*, 2016, **172**, 98.
93 M. Li, *Ionics*, 2012, **18**, 507–512.
94 F. Wang, J. Yang, Y. N. NuLi and J. L. Wang, *J. Power Sources*, 2011, **196**, 4806–4810.
95 F. Croce, A. D'Epifanio, P. Reale, L. Settimi and B. Scrosati, *J. Electrochem. Soc.*, 2003, **150**, A576–A581.
96 M. Carewska, G. Appetecchi, F. Cardellini and S. Passerini, *Solid State Ionics*, 2001, **139**, 211–218.
97 F. Zhang, S. Passerini, B. B. Owens and W. H. Smyrl, *Electrochem. Solid-State Lett.*, 2001, **4**, A221–A223.
98 P. Balaya, H. Li, L. Kienle and J. Maier, *Adv. Funct. Mater.*, 2003, **13**, 621–625.
99 J. Wu, Z. H. Li, L. Ju, D. C. Li, J. W. Zheng and Y. H. Xu, *Rare Met. Mater. Eng.*, 2013, **42**, 684–687.
100 W. B. Chen, H. S. Fang, B. Yang and W. H. Ma, *ECS Electrochem. Lett.*, 2015, **4**, A76–A78.
101 L. Dimesso, S. Jacke, C. Spanheimer and W. Jaegermann, *J. Solid State Electrochem.*, 2012, **16**, 911–919.
102 L. Dimesso, C. Spanheimer and W. Jaegermann, *J. Alloys Compd.*, 2014, **582**, 69–74.
103 L. Dimesso, C. Spanheimer, D. Becker and W. Jaegermann, *J. Eur. Ceram. Soc.*, 2014, **34**, 933–941.
104 L. Dimesso, C. Spanheimer and W. Jaegermann, *Solid State Sci.*, 2014, **30**, 89–93.
105 L. Dimesso, C. Spanheimer and W. Jaegermann, *Ionics*, 2014, **20**, 621–628.
106 L. Dimesso, D. Becker, C. Spanheimer and W. Jaegermann, *Prog. Solid State Chem.*, 2014, **42**, 184–190.
107 L. Dimesso, C. Spanheimer, M. M. Mueller, H. J. Kleebe and W. Jaegermann, *Ionics*, 2015, **21**, 2101–2107.
108 D. Di Lecce, J. Manzi, F. M. Vitucci, A. De Bonis, S. Panero and S. Brutti, *Electrochim. Acta*, 2015, **185**, 17–27.
109 L. Castro, R. Dedryvère, J.-B. Ledeuil, J. Bréger, C. Tessier and D. Gonbeau, *J. Electrochem. Soc.*, 2012, **159**, A357–A363.
110 S. Tanaka, M. Taniguchi and H. Tanigawa, *J. Nucl. Mater.*, 2000, **283**, 1405–1408.
111 K. P. Yao, D. G. Kwabi, R. A. Quinlan, A. N. Mansour, A. Grimaud, Y.-L. Lee, Y.-C. Lu and Y. Shao-Horn, *J. Electrochem. Soc.*, 2013, **160**, A824–A831.
112 H. Jadhav, S. Suryawanshi, M. More and S. Sinha, *J. Alloys Compd.*, 2018, **744**, 281–288.
113 H. Hou, Q. Peng, S. Zhang, Q. Guo and Y. Xie, *Eur. J. Inorg. Chem.*, 2005, **2005**, 2625–2630.
114 P. E. Blanchard, A. P. Grosvenor, R. G. Cavell and A. Mar, *Chem. Mater.*, 2008, **20**, 7081–7088.
115 A. W. Burns, K. A. Layman, D. H. Bale and M. E. Bussell, *Appl. Catal., A*, 2008, **343**, 68–76.
116 M. C. Biesinger, B. P. Payne, A. P. Grosvenor, L. W. Lau, A. R. Gerson and R. S. C. Smart, *Appl. Surf. Sci.*, 2011, **257**, 2717–2730.
117 B. Chowdari, K. Tan, W. Chia and R. Gopalakrishnan, *J. Non-Cryst. Solids*, 1991, **128**, 18–29.
118 L. Guo, Y. Zhao and Z. Yao, *Dalton Trans.*, 2016, **45**, 1225–1232.